Triacylphosphines as Phosphorus Sources for the Synthesis of Transition Metal Phosphide Nanoparticles

Artsiom Antanovich,[1,§*] Andrey Iodchik,[1] Jing Li,[1] Pavel Khavlyuk,[1] Volodymyr Shamraienko,[1] Vladimir Lesnyak[1,*]

[1]Physical Chemistry, TU Dresden, Zellescher Weg 19, 01069 Dresden, Germany

[§]Present address: Institute of Physical Chemistry and Electrochemistry, Leibniz University Hannover, Callinstrasse 3a, D-30167 Hannover, Germany

Abstract

Transition metal phosphide (TMP) nanoparticles (NPs) have emerged as a versatile material for a wide array of energy conversion/storage applications due to their robustness and a broad range of available compositions, stoichiometries, and crystalline structures. Combined with size and shape control, this opens many possibilities to tailor NPs' electronic, physical, and chemical properties. One of the main hurdles towards broader implementation of TMP NPs consists in their challenging synthesis further exacerbated by the limited choice of available phosphorus precursors. On the one hand, the synthesis of TMP NPs can be carried out using various alkyl- or arylphosphines, which require prolonged heating at high temperatures, while on the other hand, the use of highly reactive $P(SiMe_3)_3$, white phosphorus, or PH_3 poses additional obstacles associated with their hazardous nature, high cost, and limited availability. In this work, we report the use of acylphosphines as a new class of phosphorus sources for the synthesis of nickel and cobalt phosphide NPs. We demonstrate that they react with respective metal chlorides at moderate temperatures as low as 250 °C yielding amorphous/poorly crystalline NPs, which can later be crystallized at 305 °C. After ligand stripping with HPF_6, the prepared NPs were shown to be an effective electrocatalyst for the hydrogen evolution reaction in the acidic medium exhibiting overpotentials as low as 50 mV at a current density of 10 mA/cm², which is among the lowest overpotentials for these materials and is quite competitive to commercial platinum-based catalysts.

INTRODUCTION

Over the last decade transition metal phosphide (TMP) nanoparticles (NPs) have emerged as a material of interest for a variety of energy conversion/storage applications, such as electrical capacitors,[1,2] thermoelectrics,[3] ion batteries,[4] etc. To date, there have been many reports on the synthesis of phosphides of nickel,[5–10] cobalt,[8,9,11–13] iron,[8,14–17] molybdenum,[18–20] copper,[21–24] manganese,[25–27] tungsten,[28] etc.

One of the important rapidly developing research avenues for this class of materials is their application in various catalytic processes including photocatalysis,[29,30] organic catalysis,[31–34] electrocatalysis for CO_2-conversion,[35–39] hydrogen and oxygen evolution[40–46]. Over the years, their catalytic performance characteristics have been steadily approaching those of state-of-the-art systems based on noble metals. In addition, TMPs comprise widely abundant elements, which drastically reduces the cost of their large-scale implementation.[41,47,48] Moreover, many TMPs exhibit excellent robustness and broad flexibility of their physical, chemical, and electronic properties due to a vast number of available stoichiometries, and crystal structures, which can be further modified by alloying, doping, as well as size- and shape-control.

One of the main obstacles hindering the development of TMP catalysts is their challenging synthesis due to the strong metal-phosphorus and covalent phosphorus-phosphorus bonds, which usually require harsh reaction conditions and an appropriate phosphorus source, the range of which remains severely limited.[49] Often, such NPs are prepared on various supports at high (> 500 °C) temperatures,[50,51] which greatly increases the required energy input. The introduction of colloidal syntheses in solution helped resolve this issue and opened new possibilities to manipulate the properties of TMP NPs. The majority of works reported so far utilized either trialkyl- or triarylphosphines (e.g. trioctylphosphine)[5–7,11–14,16,21,26] or organophosphites[8–10] as a phosphorous source in combination with metal acetates,[5,23,27] chlorides,[8,19,21] acetylacetonates,[6,7,11] oxides,[15] carbonyls,[12,14,16,25,26] bulk or nanosized metals[13] at elevated temperatures.[41] However, due to the low reactivity of these phosphorus sources, the synthesis protocols still require keeping the reaction at high temperatures (albeit significantly lower than previous approaches – 300-360 °C) for prolonged periods of time and the use of large amounts of stabilizing agents such as fatty amines[5–8,13,14,16,21] or fatty acids[11,12,25]. On the other side of the reactivity spectrum are $P(SiMe_3)_3$,[25,52] white phosphorus,[53,54] and PH_3 gas,[55,56] but they pose significant hazards due to their high flammability and toxicity as well as high cost.

In this work, we report the high yield and purity synthesis of acylphosphines employing inexpensive starting materials. Using tributyrylphosphine and tribenzoylphosphine as a case study, for the first time we demonstrate their utility as a new class of reactive phosphorus precursors for the preparation of nickel, cobalt, iron, and molybdenum phosphides at moderate (250-305 °C) temperatures. We demonstrate that the size and crystallinity degree of resulting metal phosphide NPs can be controlled by the synthesis temperature and the type of acyl substitutes of the phosphine. Finally, we studied the performance of the ligand-exchanged TMP NPs as electrocatalysts for hydrogen evolution reaction (HER) in the acidic and basic media. We show that among the studied TMP NPs the lowest HER overpotential of 50 mV at 10 mA/cm^2 and a small Tafel slope of 46 mV/dec

were achieved by $Ni_2P/Ni_{12}P_5$ NPs in acidic media, which are among the best values demonstrated by non-noble metal-based TMP NPs reported to date.

EXPERIMENTAL PART

Materials

Benzoyl chloride (99.5+ %), 1,2-dimethoxyethane (DME, 99+ %, stabilized with butylated hydroxytoluene), hexane (97 %, extra dry), N-methylformamide (NMF, 99 %), sodium (≥ 99.8 %), tert-butanol (*t*-BuOH, 99.5 %), tetrahydrofuran (THF, 99.5 %, stabilized, extra dry), and sulfuric acid (95 %) were purchased from Acros. Butyryl chloride (≥ 99 %), cobalt (II) chloride (> 98 %), copper (I) chloride (≥ 99.995 %), ethyl butyrate (99 %), hexafluorophosphoric acid (HPF_6, ~55 wt. % in H_2O), iron (II) chloride (98 %), methyl benzoate (99 %), molybdenum (V) chloride (99.6 %), naphthalene (≥ 99 %), nickel (II) chloride (98 %), 1-octadecene (ODE, technical grade, 90 %), red phosphorus (powder, 99 %), and toluene (anhydrous, 99.8 %) were purchased from Sigma-Aldrich. Tri-n-octylphosphine (TOP, 97 %) was purchased from abcr. Methanol (99.8 %), n-hexane (≥ 97 %), 2-propanol (99.8 %), acetonitrile (≥ 99.95 %), and ethanol (≥ 99.8 %) were purchased from Fisher Chemical. Deuterochloroform (99,8 at. % D, stabilized with Ag) was purchased from Carl Roth. Potassium hydroxide (KOH, 90 %) was purchased from Merck. DME was dried by refluxing over sodium/benzophenone for 2 h under argon followed by distillation under argon.[57] ODE was dried and degassed under vacuum (0.1 mbar) at 90 °C for 3 h. Both solvents were stored in the nitrogen-filled glovebox over 3 Å molecular sieves.

Synthesis of tributyrylphosphine ($(PrCO)_3P$) and tribenzoylphosphine (Bz_3P)

Caution! *Synthesis of sodium phosphide involves heating highly reactive compounds in a flammable solvent, which can constitute a fire hazard. In addition, sodium phosphide readily reacts with water (including air moisture) and protic solvents (such as alcohols) with the release of toxic and explosive phosphine gas.*

Prior to use, all glassware was dried at 150 °C for 24 h. All synthesis operations were performed either in the nitrogen-filled glovebox or on a Schlenk line under an argon atmosphere. The acylphosphine synthesis procedure was adapted from ref. 58.

In the nitrogen-filled glovebox, a 100 mL three-neck flask was loaded with 3.1 g (100 mmol) of red phosphorus powder, 2.6 g (20 mmol) of naphthalene, and 80 mL of dry DME. The flask was removed from the glovebox and connected to a Schlenk line with argon atmosphere. Then 8.1 g (350 mmol) of sodium cut into small chunks were added into the flask under argon flow. Afterward, the flask was sealed with silicone septa, heated up to 80 °C, and kept stirring at this temperature overnight. During the reaction, the suspension in the flask turned from red to dark green and then black. After the reaction, the flask was cooled to room temperature and the reaction mixture was transferred via a double-tipped cannula into air-tight argon-filled glass centrifuge tubes and centrifuged at 4500 rpm

for 10 min. The supernatant was removed via cannula, the precipitate was redispersed in 30 mL of dry DME, and the mixture was centrifuged. The above redispersion-precipitation process was repeated one more time. Finally, the precipitate was redispersed in 300 mL of dry DME and transferred via a double-tipped cannula into a degassed 500 mL three-neck flask under argon.

Then the reaction mixture was cooled down with an ice bath to 0 °C and the solution of 21.2 mL (210 mmol) of *t*-BuOH in 30 mL of DME was slowly added via the syringe pump. After that, the ice bath was removed, and the flask was allowed to warm up to room temperature and kept under vigorous stirring for 2 h. Then the flask was placed in an ice bath and 19.8 mL (150 mmol) of ethyl butyrate or 18.8 mL (150 mmol) of methyl benzoate were added dropwise. The flask was kept at room temperature for 1 h, during which the reaction mixture turned greenish-yellow (in the case of butyrate) or dark red (in the case of benzoate). Afterward, the flask was cooled to 0 °C, and 30.9 mL (300 mmol) of butyryl chloride or 34.9 mL (300 mmol) of benzoyl chloride were slowly added dropwise. ***Note:*** *The reaction is highly exothermic, thus, to avoid rapid temperature rise, the rate of addition should be carefully controlled.* The reaction mixture was left under vigorous stirring overnight whilst the reaction mixture turned yellowish-grey (in the case of $(PrCO)_3P$) or yellow (in the case of Bz_3P). ***Note:*** *If the reaction mixture becomes too viscous it can be further diluted with dry DME or THF.* After that, the solids were removed from the reaction mixture by centrifugation under an argon atmosphere yielding a transparent solution. Then all volatiles were evaporated from the reaction mixture under vacuum resulting in yellow oil ($(PrCO)_3P$) or bright yellow powder (Bz_3P).

To purify $(PrCO)_3P$, the reaction product was diluted two times with hexane, centrifuged under argon to remove remaining solids, and then kept under a vacuum on a Schlenk line at 30 °C for 8 h. For the purification of Bz_3P, the reaction product was dissolved under an inert atmosphere in 100 mL of dry THF and then precipitated by adding ca. 300 mL of dry hexane. The solid was isolated by centrifugation and recrystallized one more time as described in the previous sentence. Finally, the solid product was dried under a vacuum at room temperature for 8 h.

$(PrCO)_3P$: ^{1}H NMR (300 MHz, $CDCl_3$) δ 2.86 (td, J = 7.2, 1.7 Hz, 6H, CH_2-CO), 1.64 (h, J = 7.3 Hz, 6H, CH_3-CH_2), 0.93 (t, J = 7.4 Hz, 9H, CH_3). **^{13}C NMR** (75 MHz, $CDCl_3$) δ 215.2 (d, $^1J_{PC}$ = 49.3 Hz, C=O), 50.8 (d, CH$_2$-CO, $^2J_{PC}$ = 30.9 Hz), 17.2 (d, CH_3-CH_2 $^3J_{PC}$ = 3.6 Hz), 13.5 (CH_3, s). **^{31}P NMR** (121 MHz, $CDCl_3$): δ = 61.3 ppm (s).

Elemental analysis: calculated for $C_{12}H_{21}O_3P$: C, 59.00; H 8.67; found: C, 58.70; H 8.86.

Bz_3P: ^{1}H NMR (300 MHz, $CDCl_3$) δ 8.05 – 7.95 (m, 6H, *o*-H), 7.65 – 7.56 (m, 3H, *p*-H), 7.53 – 7.45 (m, 6H, *m*-H). **^{13}C NMR** (75 MHz, $CDCl_3$) δ 206.0 (d, $^1J_{PC}$ = 33.3 Hz, C=O), 140.2 (d, $^2J_{PC}$ = 34.6 Hz, C_{ipso}), 134.2 (d, J = 1.4 Hz, C_{para}), 129.0 – 128.6 (m, C_{arom}). **^{31}P NMR** (121 MHz, $CDCl_3$): δ = 54.0 ppm (s).

Elemental analysis: calculated for $C_{21}H_{15}O_3P$: C, 72.82; H 4.37; found: C, 72.88; H 4.28.

Synthesis of nickel, cobalt, iron, copper, and molybdenum phosphide NPs

In a typical synthesis, 0.5 mmol of metal chloride were mixed with 900 μL of TOP (2 mmol) and 5 mL of dry degassed ODE in a nitrogen-filled glovebox. The obtained mixture was transferred to a Schlenk line, heated under argon flow to 170 °C, and maintained at this temperature for 15 min to dissolve the metal precursor. After that, the solution was cooled down to 90 °C, degassed under vacuum (0.1 mbar) for 30 min, and then purged with argon. In parallel, in a nitrogen-filled glovebox, a phosphorus precursor solution was prepared by dissolving either 67.5 μL (0.25 mmol) of $(PrCO)_3P$ in 1 mL of dry degassed ODE or 86.5 mg of Bz_3P (0.25 mmol) in 1 mL of anhydrous toluene. Next, the obtained solution was injected into the metal precursor solution, and the flask was evacuated for 5 min to remove the solvent. Then, the temperature was quickly increased to the required temperature (250 °C, 275°C, or 305 °C) and kept for 25 min (in the case of molybdenum phosphide for 2 h) for the nucleation and growth of NPs. Finally, the reaction mixture was cooled down to room temperature, and NPs were purified by multiple precipitation and redispersion steps, using a 2-propanol/methanol mixture (2:1) and hexane.

Ligand stripping

Organic ligands on the surface of metal phosphide NPs were displaced using HPF_6. The removal of ligands was performed by adding 4 mL of NMF and 10 μL of ~55 wt. % HPF_6 aqueous solution to a 4 mL solution of NPs in hexane. The mixture was vigorously stirred for 30 min followed by adding 10 μL of HPF_6 solution and stirring for 30 min. Afterward, the hexane layer was discarded, and NPs were purified by the multiple precipitations with a toluene/acetonitrile mixture (5:1) and redispersing in NMF. Finally, the NPs were redispersed in ethanol and stored prior to the electrocatalytic tests.

Characterization

^{1}H, ^{13}C, and ^{31}P NMR spectroscopy was performed using Bruker Avance III 600 spectrometer. For the measurements, acylphosphines (ca. 5 w/v %) were dissolved in deuterochloroform in the nitrogen-filled glovebox and transferred into air-tight NMR tubes. Elemental analysis (CHNS) was done with FlashSmart Elemental Analyzer.

Bright-field transmission electron microscopy (TEM) imaging was performed on a JEOL JEM-1400 Plus microscope operated at 120 kV. Powder X-ray diffraction (XRD) patterns were acquired using a Bruker D2 Phaser equipped with an X-ray tube with a Cu anode operated at 30 kV and 10 mA. WinXPow software with references from the Inorganic Crystal Structure Database (ICSD) was used for the phase analysis. For the measurements, concentrated hexane solutions of metal phosphide NPs were drop-cast on a Si wafer and dried under air. Fourier-transform infrared spectroscopy (FTIR) measurements were performed on a Nicolet 8700 FTIR spectrometer using the attenuated total reflectance (ATR) method.

Electrochemical tests were conducted using a three-electrode measurement setup (Metrohm Autolab) to characterize the catalytic performance of the synthesized materials. The experimental arrangement comprised a reference electrode, a counter electrode, and a working electrode. For the experiments conducted in 0.5 M H_2SO_4, an Ag/AgCl electrode in saturated KCl was employed as the reference electrode. For experiments in 1 M KOH, a Hg/HgO electrode served as the reference electrode. A graphite rod was utilized as the counter electrode. A glassy carbon disk electrode, with a diameter of 3 mm and a geometric area of 0.07 cm^2 was used as a working electrode. The NP films were deposited by drop-casting aliquots of the ethanol dispersions of ligand-stripped NPs onto the glassy carbon electrode to get an average mass loading of 0.5 – 0.7 mg/cm^2. After drying in ambient air, a stable and uniform catalyst layer on the electrode surface was formed. The electrochemical measurements were conducted through linear sweep voltage scans initiated from -0.4 to 0 V in 0.5 M H_2SO_4 and -0.6 to 0 V in 1 M KOH *vs.* the reversible hydrogen electrode with a scan rate of 5 mVs^{-1}.

RESULTS AND DISCUSSION

$(PrCO)_3P$ and Bz_3P were synthesized by the acylation of sodium dihydrogenphosphide prepared by the protonation of sodium phosphide with *t*-BuOH (**Scheme 1**). The composition and structure of these compounds were confirmed by elemental analysis and NMR-spectra (**Figure S1** in the Supporting Information), which were consistent with the literature data.[58,59] Both phosphines were isolated with high (> 50 %) reaction yields and purity and were found to be soluble in THF, DME, $CHCl_3$, and toluene. In addition, $(PrCO)_3P$ is also soluble in hexane and ODE. When exposed to air, $(PrCO)_3P$ reacts exothermically producing white fumes, while Bz_3P was found to be relatively stable.

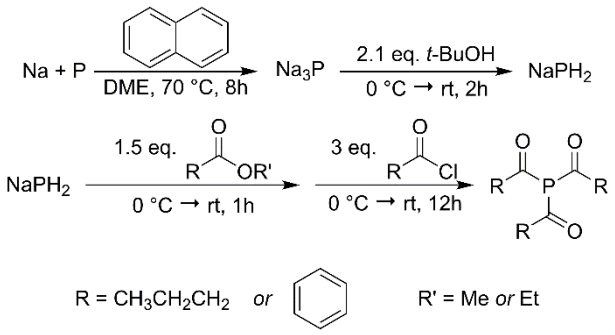

Scheme 1. Synthesis scheme of $(PrCO)_3P$ and Bz_3P.

Metal phosphide NPs were synthesized by reacting metal chlorides with either $(PrCO)_3P$ or Bz_3P as a phosphorus precursor in ODE. To investigate the reactivity of the prepared phosphines we used the heat-up approach widely applied in the synthesis of TMP NPs. During the preliminary experiments the phosphines were found to be unreactive towards nickel and cobalt oleates in ODE prior to their decomposition; $(PrCO)_3P$ quickly decomposed when using respective chlorides in oleylamine, whereas Bz_3P was more stable but led to the low yield and irregular shaped NPs. Thus, instead, we opted to perform the synthesis in ODE using TOP as a metal complexing agent facilitating

the dissolution of respective chlorides. After the dissolution of metal precursors, the acylphosphines were injected at 90 °C into the reaction mixture, which was then heated up to the required temperature (250 – 305 °C). Upon heating the reaction mixture began darkening at ca. 150 °C and 170 °C in the case of $NiCl_2$ and $CoCl_2$, respectively, indicating the reaction between acylphosphines and metal salts and kept turning black over the reaction progress.

Figure 1 shows TEM images and XRD patterns of nickel phosphide NPs prepared using the synthesized acylphosphines. One can see that at 250 °C both phosphorus sources yield small (5 ± 1 nm and 4 ± 0.5 nm, in the case of Bz_3P and $(PrCO)_3P$, respectively) quasi-spherical NPs. Corresponding XRD patterns exhibit significantly broadened low-intensity reflexes attributed to the hexagonal Ni_2P phase consistent with small-sized poorly crystalline NPs. When the synthesis temperature is increased to 305 °C, the size of obtained NPs increases to 8.5 ± 1.5 nm and 7.5 ± 1.5 nm in the case of Bz_3P and $(PrCO)_3P$, respectively, while the XRD reflections become more pronounced, in line with previous reports suggesting that TMP NPs require high temperature to crystallize.[8,60,61] It is worth mentioning that higher temperatures resulted in higher NP yields indicating that crystallization was accompanied by further monomer conversion facilitating the size increase.

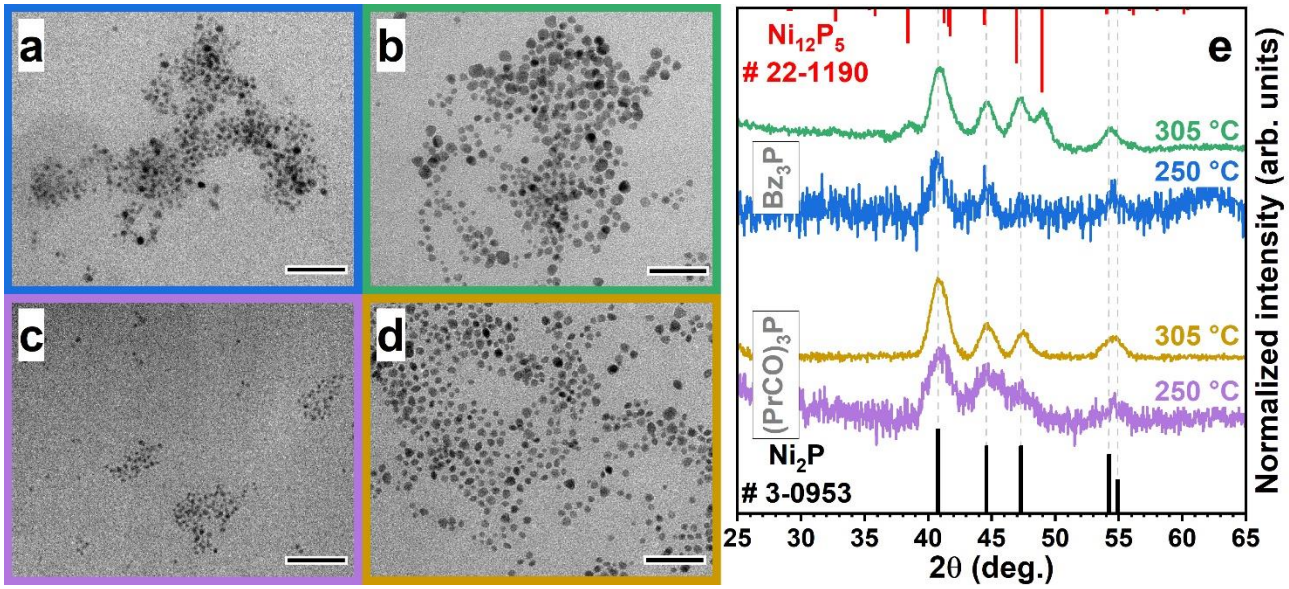

Figure 1. TEM images (a–d) and XRD patterns (e) of nickel phosphide NPs synthesized using Bz_3P (a – 250 °C, b – 305 °C) and $(PrCO)_3P$ (c – 250 °C, d – 305 °C) at different temperatures. Scale bars in TEM images are 50 nm. Dashed lines in (e) correspond to the XRD pattern of hexagonal Ni_2P (# 3-0953) and serve as a guide for an eye.

Furthermore, nickel phosphide NPs prepared with Bz_3P at 305 °C exhibit additional reflections at 38.5° and 49.0° attributable to the metal-rich tetragonal $Ni_{12}P_5$ phase. Its formation might be explained by the lower reactivity of the acylphosphine as suggested by its aforementioned stability towards air exposure and its higher thermal stability.[58] Considering the mechanistic speculations

above, lower reactivity results in a smaller yield of poorly crystalline intermediates leaving more unreacted nickel salt in solution, creating more metal-rich conditions for later reaction stages, which were previously reported to facilitate the formation of $Ni_{12}P_5$ NPs.[7] Such an assumption is also in line with the slightly bigger size of NPs prepared with Bz_3P, since slower monomer flux generally facilitates the growth of NPs to larger sizes.

In a similar manner to nickel phosphide, we also synthesized cobalt phosphide NPs using cobalt dichloride as a metal source. Cobalt precursor was found to be slightly less reactive towards acylphosphines, thus low-temperature cobalt phosphide was prepared at 275 °C. TEM images and corresponding XRD patterns of the prepared cobalt phosphide NPs are displayed in **Figure 2**.

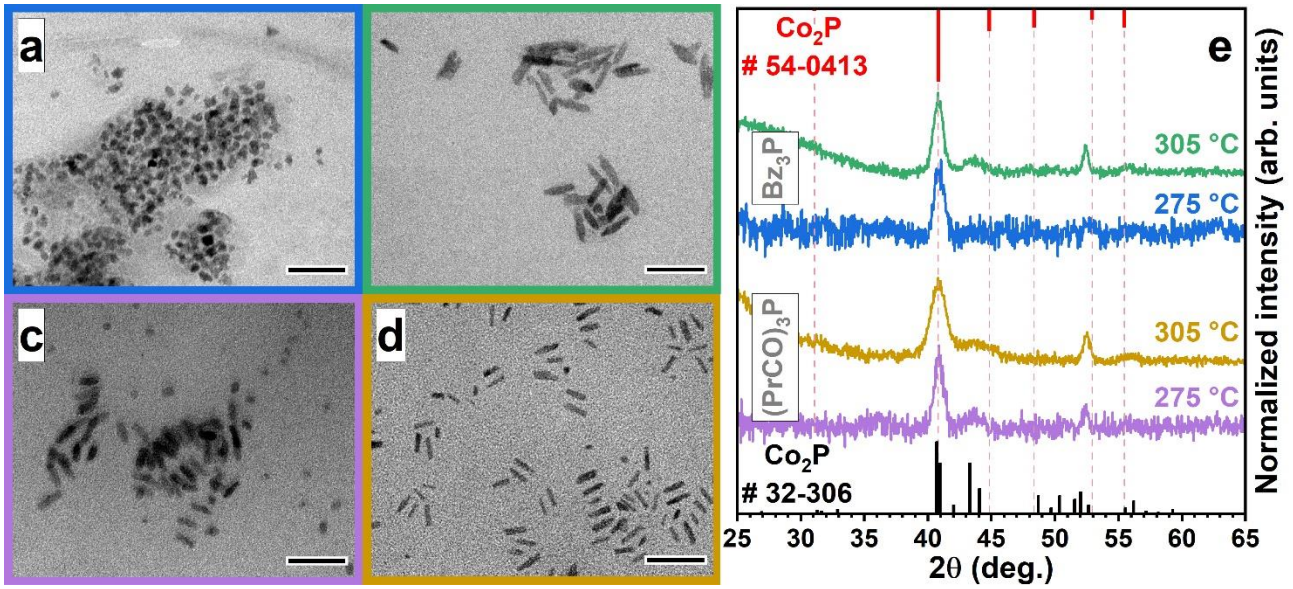

Figure 2. TEM images (a-d) and XRD patterns (e) of cobalt phosphide NPs synthesized using Bz_3P (a – 275 °C, b – 305 °C) and $(PrCO)_3P$ (c – 275 °C, d – 305 °C) at different temperatures. Scale bars in TEM images are 50 nm. Dashed lines in (e) correspond to the XRD pattern of hexagonal Co_2P (# 54-0413) and serve as a guide for an eye.

As in the case of Ni phosphides, cobalt phosphide NPs synthesized using Bz_3P at lower temperatures are quasi-spherical albeit having rougher surface with average sizes of 9 ± 1.5 nm. At the same time, in the case of $(PrCO)_3P$) a mixture of rod-like (length 19.0 ± 2.5 and width 7.5 ± 1.0 nm) and quasi-spherical NPs (7.5 ± 2 nm) are observed (**Figure 2c** and **Figure S2** in the Supporting Information). In both cases, respective XRD patterns exhibit low-intensity reflections of orthorhombic Co_2P. The syntheses at higher temperatures result in cobalt phosphide NPs with markedly different shapes of nanorods with dimensions of 18 ± 3 nm × 5 ± 1 nm and 29 ± 4.5 nm × 6.5 ± 1 nm when using $(PrCO)_3P$ and Bz_3P, respectively. Notably, the diameter of cobalt phosphide nanorods is smaller than the diameter of quasi-spherical NPs prepared at lower temperatures, indicating that some recrystallization of smaller NPs takes place at higher temperatures, which is consistent with the NP growth mechanistic speculations above. Similarly to Ni phosphides, the

increase of synthesis temperature also facilitates the increase of NP crystallinity as evidenced by a higher intensity of XRD reflections as well as the appearance of additional reflection at ~52.4°.

It is worth mentioning that TMP NPs prepared with alkyl- or arylphosphines in metal-rich conditions often exhibit hollow structures due to the two-step reaction mechanism involving phosphidation of intermediate metallic NPs leading to the appearance of voids due to the Kirkendall effect.[12,60–63] The formation of holes in NPs can be suppressed by significantly increasing the ratio of alkylphosphines above ca. 9-fold excess of phosphorus precursor, which pushes the reaction towards the formation of amorphous metal phosphide NPs.[60,61] In our case, particles appear solid and homogeneous and we did not observe any signs of the formation of metallic NPs at any point of the reaction. This suggests that even in metal-rich conditions acylphosphines with molecular structure similar to the abovementioned alkyl- or arylphosphines react with metal salts, directly forming respective poorly crystalline or amorphous phosphide NPs, which later recrystallize and provide the flux of monomers for further NP growth explaining the larger sizes and the shape change of NPs prepared at higher temperatures. Together with somewhat lower reaction temperatures, this suggests that the introduction of the carbonyl group in the vicinity of the central phosphorus atom significantly improves the reactivity of phosphines.

Furthermore, we also examined the reactivity of the prepared phosphines towards copper (I), iron (II), and molybdenum (V) chlorides. In the case of copper and iron, TEM imaging reveals the formation of very large crystalline NPs of the respective phosphides with sizes on the scale of hundreds of nm (see **Figure S3**). Such drastic size difference can be most likely attributed to the poor ability of chloride and TOP to passivate the surface of the formed metal phosphide NPs, resulting in their uncontrolled growth. Conversely, the reaction with molybdenum (V) chloride yielded very small (~2 nm) amorphous NPs with poorly defined shapes (see **Figure S3 d,h**). It is worth mentioning that crystalline molybdenum phosphide is notoriously hard to prepare via the synthesis in solution since its crystallization requires temperatures well above 305 °C and is usually conducted as an additional annealing step.[8,18]

Since both acylphosphines and TOP can potentially act as a phosphorus source for TMP NPs, to verify whether $(PrCO)_3P$ and Bz_3P are indeed playing the major role in the reaction, we performed additional syntheses in the same manner, except for the injection of the acylphosphines. In the case of cobalt and nickel chlorides, the reaction resulted in respective phosphide NPs with poor chemical yield, however, their TEM images are markedly different from the ones shown above, demonstrating particles with significantly larger sizes of tens of nm (**Figure S4**). In the case of copper, iron, and molybdenum chlorides, no reaction was observed even after the prolonged heating at 305 °C.

Next, we evaluated the electrocatalytic performance of the synthesized NPs deposited onto the glassy carbon electrode in both acidic (0.5 M H_2SO_4) and alkaline (1 M KOH) aqueous solutions.

Since NPs synthesized in the organic medium are sterically stabilized in solution by bulky organic ligands, which can block access to active catalytic sites and severely hinder the charge transfer between/from NPs in solid film,[64–67] we first assessed the effect of ligand removal from NPs' surface on their electrocatalytic performance. Often the ligand removal from the surface of TMPs is conducted by annealing at high temperatures in a vacuum or hydrogen atmosphere,[5,7] which aside from being energy-intensive can also contaminate the film with carbonaceous residues as well as cause the unwanted phase change and particle fusion, thus severely reducing the surface area and hence the activity of the catalyst.[18,68,69] Since one of our aims was also to compare HER performance of poorly vs well-crystallized NPs, instead, we conducted an NPs' phase transfer from hexane to NMF using HPF_6, which, albeit being much milder, was shown to be effective at the removal of the native ligands from NPs leaving behind positively charged metal sites.[8,9,67,70] As illustrated in **Figure S5**, the ligand stripping from the surface of nickel phosphide NPs results in a marked overpotential drop, indicating a notable enhancement of the catalytic performance. This improvement underscores the significance of ligand choice in optimizing electron transfer and, consequently, enhancing the overall catalytic efficiency, hence, we utilized the same protocol for other TMP NP samples.

To monitor the efficiency of the ligand-exchange process, we utilized FTIR-spectroscopy (**Figure 3**). One can see that prior to ligand exchange, all samples exhibit a group of intensive bands around 2800 – 3000 cm^{-1} corresponding to symmetric and asymmetric vibrations of methyl and methylene units of long alkyl chains.[71] At the same time, we observed no sharp and intensive features at 1500 – 1700 cm^{-1} of carboxylate or carbonyl vibrations,[72] which might have appeared due to the presence of unreacted acylphosphines or by-products of their decomposition, thus suggesting that TOP acts as a sole organic surface ligand. After adding HPF_6 into the biphasic mixture and vigorously shaking it for 1 min the hexane phase became colorless, and the NPs quickly migrated to the NMF layer indicating the removal of organic species from the NPs' surface. Successful ligand stripping is also confirmed by FTIR data, where we observe the complete or nearly complete disappearance of alkyl chain vibration signals (**Figure 3**). Notably, during and after the phase transfer some of the amorphous samples exhibited lower colloidal stability than their crystalline counterparts thus complicating complete ligand stripping even after the addition of another HPF_6 aliquot, which in turn explains weak residual signals of organic ligands. This can be explained by the less defined surface of amorphous NPs potentially exposing more sites, which poorly adsorb protons or neutralize their charge, thus negating their contribution to colloidal stability.

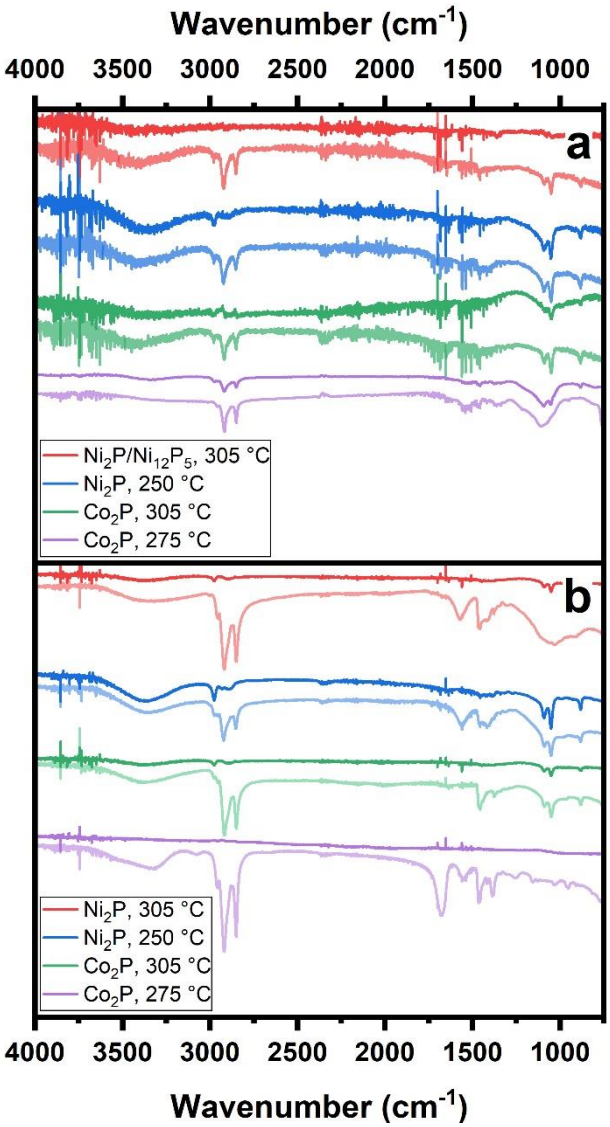

Figure 3. FTIR-ATR spectra of nickel and cobalt phosphide NPs synthesized using Bz_3P (a) and $(PrCO)_3P$ (b) before (light lines) and after (darker lines) ligand exchange with HPF_6.

Figure 4 a,b presents the linear sweep voltammetry (LSV) curves of cobalt and nickel phosphide NPs recorded in 0.5 M H_2SO_4 aqueous solution and exhibits two clear trends. First, the overpotentials of nickel phosphide NPs are lower than those of cobalt phosphide NPs, which can be explained by the lower Gibbs free energy of the adsorbed atomic hydrogen ΔG_{H^*} indicating the ability of the catalyst to release hydrogen and unblock the reactive catalytic sites.[9] Second, the samples with lower crystallinity prepared at lower temperatures demonstrate markedly higher overpotentials than their counterparts prepared at 305 °C with more pronounced crystalline features in XRD patterns, which can be explained by the much higher conductivity of well-crystallized NPs.[73] In the case of high-temperature nickel phosphide NPs synthesized using Bz_3P and $(PrCO)_3P$, overpotentials of only 50 mV and 68 mV, respectively, are required to reach a current density of 10 mA/cm², which favorably compares against the reported nickel and cobalt phosphides (see **Table S1** and **Figure S6**

in the Supporting Information) and is a quite competitive value compared to Pt/C (28 mV) employed as a commercial catalyst.

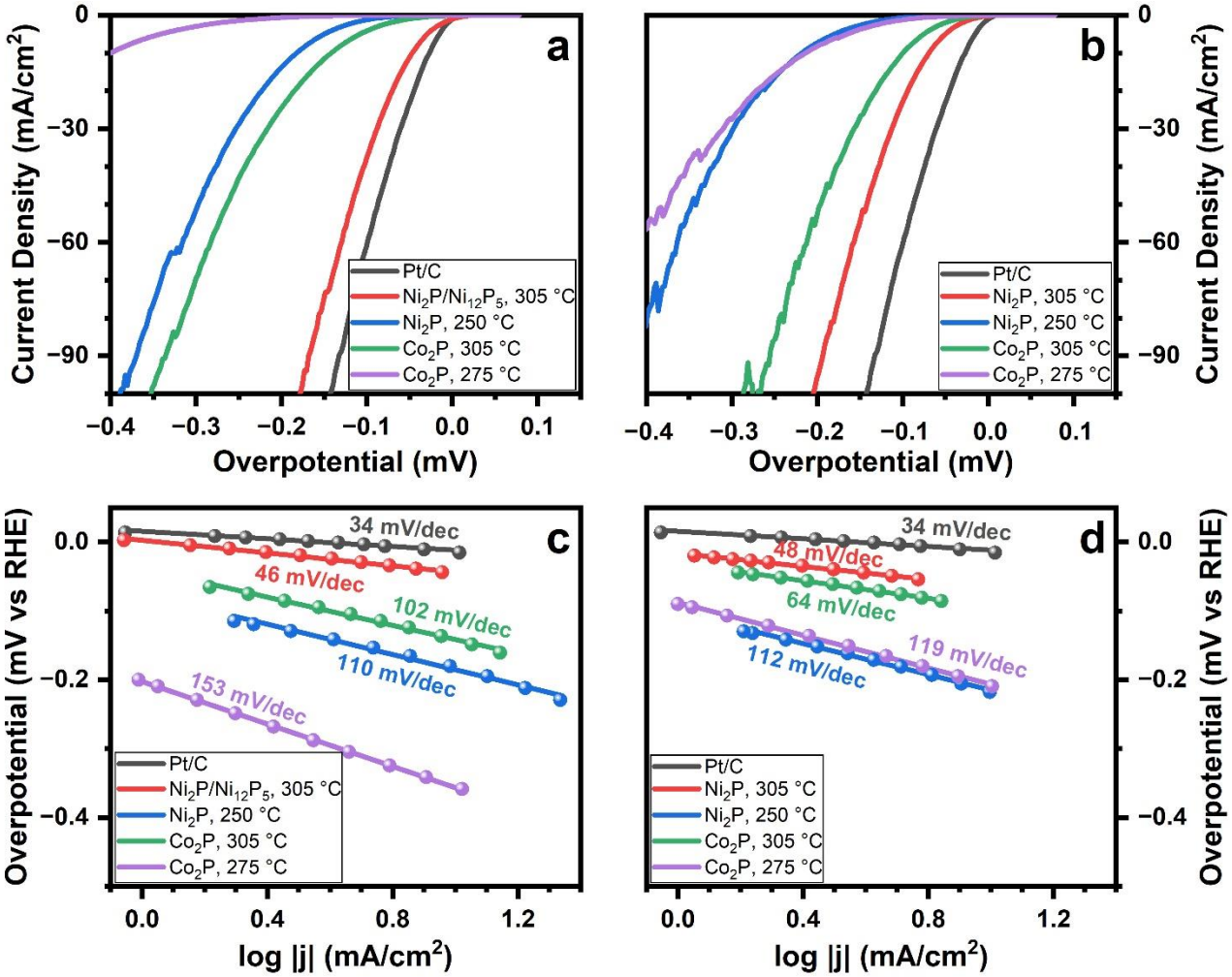

Figure 4. HER-performance of NPs in 0.5 M H_2SO_4: LSV curves (a, b) and Tafel plots (c, d) of the metal phosphide NPs synthesized with Bz_3P (a, c) and $PrCO_3P$ (b, d).

Currently, there is limited information in the literature, directly comparing the catalytic performance of amorphous and crystalline nickel and cobalt phosphide NPs, since they can usually be accessed via different synthetic routes, which results in dissimilar compositions, sizes, and structures further complicating proper comparison. In this regard, our work enables the examination of the effect of crystallinity degree on the electrocatalytic performance of TMPs prepared via similar routes and possessing comparable parameters. Although more sophisticated studies, which go beyond the scope of this paper, are needed to properly examine the underlying processes involved in the electrocatalysis, we are still able to draw some qualitative conclusions.

In general, amorphous materials are expected to be beneficial for catalysis because they can offer a more flexible composition and structure as well as owing to disorder introducing more defects and vacancies often presumed to be electrocatalytically active sites.[40,69,74,75] On the other hand, crystalline NPs might exhibit better performance since they possess well-defined facets and some

specific crystallographic planes were shown to be particularly active in the reduction of hydrogen in water molecules.[5,76,77] Furthermore, films of crystalline NPs have higher electrical conductivity, which appears to be the major factor contributing to the better catalytic performance of crystalline NPs compared to amorphous ones.[78]

To further assess the catalytic efficiency, Tafel slope analysis was conducted, serving as an indicator of the reaction kinetics. As illustrated in **Figure 4 c,d** crystalline nickel phosphide NPs exhibit the smallest Tafel slopes (46 and 48 mV/dec in the case of Bz_3P and $(PrCO)_3P$, respectively) compared to amorphous/poorly crystalline nickel phosphide (112 and 110 mV/dec), crystalline (102 and 64 mV/dec) and amorphous/poorly crystalline (145 and 118 mV/dec) cobalt phosphide NPs. These values do not match the Tafel slope values of 29, 38, and 116 mV/dec expected for particular rate-limiting steps of the Volmer-Heyrovsky-Tafel HER mechanism, which is quite common for non-metal materials.[79] In some publications, values lower than ca. 60 mV/dec are interpreted as a probable signature of a barrierless electron transfer mechanism[80] or a mechanism involving a fast Volmer step followed by the Heyrovsky step determining the overall reaction rate.[7,45] However, more recently it was suggested that such Tafel analysis does not accurately describe electrocatalysis and does not allow conclusive identification of the rate-determining steps possibly due to more complex reaction mechanisms and altered parameter values used in theoretical calculations.[79,81] Nevertheless, a conclusion can be made that smaller Tafel slopes indicate a less hindered HER process with superior charge transfer efficiency and faster reaction kinetics.[41]

Figure 5 presents the LSV curves along with corresponding Tafel plots of cobalt and nickel phosphide NPs recorded in 1 M KOH. In general, HER overpotentials for a variety of electrocatalysts of different nature are significantly higher than those observed in the acidic solutions, most likely due to the overall change of the HER mechanism resulting in more complicated kinetics involving additional water dissociation step.[82] As one can notice, in our case we observe the same trend both in LSV curves and respective Tafel slopes across all studied electrodes pointing to slower reaction rates.

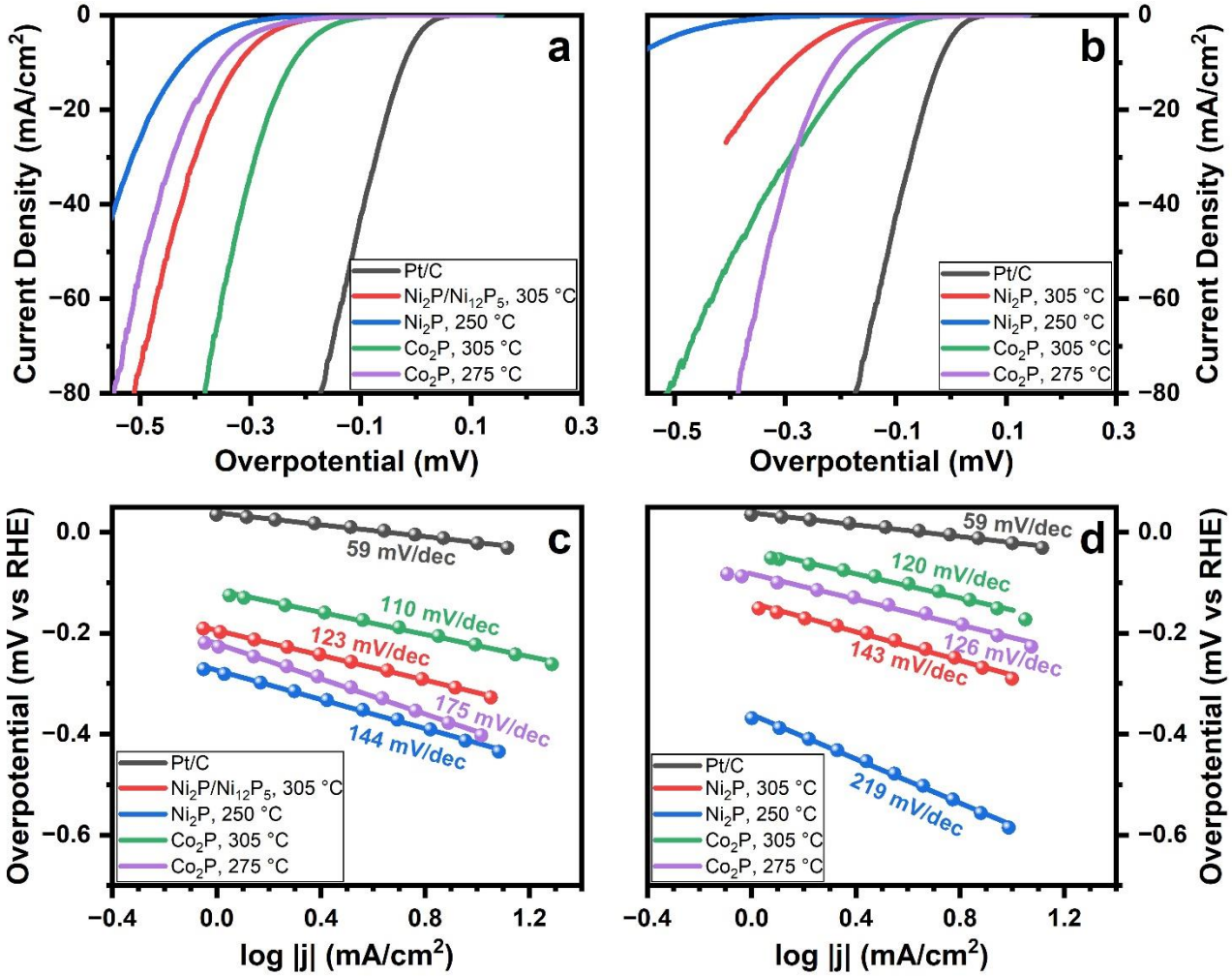

Figure 5. HER-performance of NPs in 1.0 M KOH: LSV curves (a, b) and Tafel plots (c, d) of the metal phosphide NPs synthesized with Bz_3P (a, c) and $PrCO_3P$ (b, d).

Similarly to HER in an acidic medium, lower overpotentials were achieved in the case of well-crystallized NPs further supporting our assumption that film conductivity plays an important role in the catalyst activity. Interestingly, in an alkaline medium both types of cobalt phosphide NPs exhibit lower overpotentials, which is in line with previous reports and might be attributed to the different absorbed species involved in the initial reaction steps, their binding affinity to the surface, as well as phase/compositional transformation during the electrocatalysis.[83,84]

CONCLUSIONS

In this work, we report the application of triacylphosphines as the new type of phosphorus precursors for the synthesis of nickel and cobalt phosphide NPs. We demonstrate that in comparison to alkyl- or arylphosphines with similar structures commonly used for the preparation of TMP NPs, acylphosphines possess higher reactivity towards metal chlorides and directly yield metal phosphide NPs without the intermediate metal reduction step. At the same time, they are relatively safe for use in contrast to other highly reactive phosphorus sources, such as white phosphorus, PH_3, or $P(SiMe_3)_3$.

Acylphosphines were shown to react with nickel and cobalt chlorides in the presence of TOP serving both as a cosolvent for metal precursors and a ligand for NPs at temperatures as low as 250 °C yielding NPs with sizes < 10 nm, which can later be transformed into crystalline NPs by heating up to 305 °C. This provides access to TMP NPs with different crystallinity expanding the possibility to control physical and electrical properties, which, as demonstrated in this work, determine their performance in electrocatalysis. We examined the HER performance of the synthesized Ni and Co phosphide NPs after ligand stripping using HPF_6 and showed that both types of crystalline NPs demonstrate lower overpotential than their amorphous counterparts. At the same time, in an acidic medium nickel phosphide NPs exhibit significantly better HER performance than cobalt phosphides, reaching overpotentials as low as 50 mV at a current density of 10 mA/cm², which is among the lowest overpotentials for this type of materials and can be considered as a quite competitive value compared with Pt/C (28 mV).

ASSOCIATED CONTENT

Supporting Information: ^{1}H, ^{13}C, and ^{31}P NMR spectra of the acylphosphines, additional TEM images, XRD, and electrochemistry data.

AUTHOR INFORMATION

Corresponding authors

artsiom.antanovich@pci.uni-hannover.de, vladimir.lesnyak@tu-dresden.de

Notes

The authors declare no competing financial interest.

ACKNOWLEDGMENTS

A.A. acknowledges funding from the European Union's Horizon 2020 research and innovation programme under the Marie Sklodowska-Curie grant agreement No 101031243. V.S. and P.K. thank the German Research Foundation for funding through CRC 1415, EY 16/30-1 and RTG 2767 projects. We are grateful to Heike Trepte and Anett Rudolph for the elemental analysis and NMR spectroscopy of acylphosphines.

REFERENCES

(1) Li, G.; Feng, Y.; Yang, Y.; Wu, X.; Song, X.; Tan, L. Recent Advances in Transition Metal Phosphide Materials: Synthesis and Applications in Supercapacitors. *Nano Mater. Sci.* **2023**. https://doi.org/10.1016/j.nanoms.2023.03.003.

(2) Patil, S. S.; Patil, P. S. Status Review of Nickel Phosphides for Hybrid Supercapacitors. *Nanoscale* **2022**, *14* (45), 16731–16748. https://doi.org/10.1039/D2NR05139G.

(3) Pöhls, J.-H.; Faghaninia, A.; Petretto, G.; Aydemir, U.; Ricci, F.; Li, G.; Wood, M.; Ohno, S.; Hautier, G.; Snyder, G. J.; Rignanese, G.-M.; Jain, A.; White, M. A. Metal Phosphides as Potential Thermoelectric Materials. *J. Mater. Chem. C* **2017**, *5* (47), 12441–12456. https://doi.org/10.1039/C7TC03948D.

(4) Chang, G.; Zhao, Y.; Dong, L.; Wilkinson, D. P.; Zhang, L.; Shao, Q.; Yan, W.; Sun, X.; Zhang, J. A Review of Phosphorus and Phosphides as Anode Materials for Advanced Sodium-Ion Batteries. *J. Mater. Chem. A* **2020**, *8* (10), 4996–5048. https://doi.org/10.1039/C9TA12169B.

(5) Popczun, E. J.; McKone, J. R.; Read, C. G.; Biacchi, A. J.; Wiltrout, A. M.; Lewis, N. S.; Schaak, R. E. Nanostructured Nickel Phosphide as an Electrocatalyst for the Hydrogen Evolution Reaction. *J. Am. Chem. Soc.* **2013**, *135* (25), 9267–9270. https://doi.org/10.1021/ja403440e.

(6) Cao, S.; Chen, Y.; Wang, C.-J.; He, P.; Fu, W.-F. Highly Efficient Photocatalytic Hydrogen Evolution by Nickel Phosphide Nanoparticles from Aqueous Solution. *Chem. Commun.* **2014**, *50* (72), 10427. https://doi.org/10.1039/C4CC05026F.

(7) Pan, Y.; Liu, Y.; Zhao, J.; Yang, K.; Liang, J.; Liu, D.; Hu, W.; Liu, D.; Liu, Y.; Liu, C. Monodispersed Nickel Phosphide Nanocrystals with Different Phases: Synthesis, Characterization and Electrocatalytic Properties for Hydrogen Evolution. *J. Mater. Chem. A* **2015**, *3* (4), 1656–1665. https://doi.org/10.1039/C4TA04867A.

(8) Liu, J.; Meyns, M.; Zhang, T.; Arbiol, J.; Cabot, A.; Shavel, A. Triphenyl Phosphite as the Phosphorus Source for the Scalable and Cost-Effective Production of Transition Metal Phosphides. *Chem. Mater.* **2018**, *30* (5), 1799–1807. https://doi.org/10.1021/acs.chemmater.8b00290.

(9) Liu, J.; Wang, Z.; David, J.; Llorca, J.; Li, J.; Yu, X.; Shavel, A.; Arbiol, J.; Meyns, M.; Cabot, A. Colloidal $Ni_{2-x}Co_xP$ Nanocrystals for the Hydrogen Evolution Reaction. *J. Mater. Chem. A* **2018**, *6* (24), 11453–11462. https://doi.org/10.1039/C8TA03485K.

(10) Andaraarachchi, H. P.; Thompson, M. J.; White, M. A.; Fan, H.-J.; Vela, J. Phase-Programmed Nanofabrication: Effect of Organophosphite Precursor Reactivity on the Evolution of Nickel and Nickel Phosphide Nanocrystals. *Chem. Mater.* **2015**, *27* (23), 8021–8031. https://doi.org/10.1021/acs.chemmater.5b03506.

(11) Zhang, S.; Ye, E.; Liu, S.; Lim, S. H.; Tee, S. Y.; Dong, Z.; Han, M. Temperature and Chemical Bonding-Directed Self-Assembly of Cobalt Phosphide Nanowires in Reaction Solutions into Vertical and Horizontal Alignments. *Adv. Mater.* **2012**, *24* (32), 4369–4375. https://doi.org/10.1002/adma.201201618.

(12) Popczun, E. J.; Read, C. G.; Roske, C. W.; Lewis, N. S.; Schaak, R. E. Highly Active Electrocatalysis of the Hydrogen Evolution Reaction by Cobalt Phosphide Nanoparticles. *Angew. Chemie Int. Ed.* **2014**, *53* (21), 5427–5430. https://doi.org/10.1002/anie.201402646.

(13) Callejas, J. F.; Read, C. G.; Popczun, E. J.; McEnaney, J. M.; Schaak, R. E. Nanostructured Co_2P Electrocatalyst for the Hydrogen Evolution Reaction and Direct Comparison with Morphologically Equivalent CoP. *Chem. Mater.* **2015**, *27* (10), 3769–3774. https://doi.org/10.1021/acs.chemmater.5b01284.

(14) Callejas, J. F.; McEnaney, J. M.; Read, C. G.; Crompton, J. C.; Biacchi, A. J.; Popczun, E. J.; Gordon, T. R.; Lewis, N. S.; Schaak, R. E. Electrocatalytic and Photocatalytic Hydrogen Production from Acidic and Neutral-pH Aqueous Solutions Using Iron Phosphide Nanoparticles. *ACS Nano* **2014**, *8* (11), 11101–11107. https://doi.org/10.1021/nn5048553.

(15) Chung, D. Y.; Jun, S. W.; Yoon, G.; Kim, H.; Yoo, J. M.; Lee, K.-S.; Kim, T.; Shin, H.; Sinha, A. K.; Kwon, S. G.; Kang, K.; Hyeon, T.; Sung, Y.-E. Large-Scale Synthesis of Carbon-Shell-Coated FeP Nanoparticles for Robust Hydrogen Evolution Reaction Electrocatalyst. *J. Am. Chem. Soc.* **2017**, *139* (19), 6669–6674. https://doi.org/10.1021/jacs.7b01530.

(16) Park, Y.; Kang, H.; Hong, Y.; Cho, G.; Choi, M.; Cho, J.; Ha, D.-H. Influence of the Phosphorus Source on Iron Phosphide Nanoparticle Synthesis for Hydrogen Evolution Reaction Catalysis. *Int. J. Hydrogen Energy* **2020**, *45* (57), 32780–32788. https://doi.org/10.1016/j.ijhydene.2020.03.051.

(17) D'Accriscio, F.; Schrader, E.; Sassoye, C.; Selmane, M.; André, R. F.; Lamaison, S.; Wakerley, D.; Fontecave, M.; Mougel, V.; Le Corre, G.; Grützmacher, H.; Sanchez, C.; Carenco, S. A Single Molecular Stoichiometric P-Source for Phase-Selective Synthesis of Crystalline and Amorphous Iron Phosphide Nanocatalysts. *ChemNanoMat* **2020**, *6* (8), 1208–1219. https://doi.org/10.1002/cnma.202000198.

(18) McEnaney, J. M.; Crompton, J. C.; Callejas, J. F.; Popczun, E. J.; Biacchi, A. J.; Lewis, N. S.; Schaak, R. E. Amorphous Molybdenum Phosphide Nanoparticles for Electrocatalytic Hydrogen Evolution. *Chem. Mater.* **2014**, *26* (16), 4826–4831. https://doi.org/10.1021/cm502035s.

(19) Zhang, X.; Yu, X.; Zhang, L.; Zhou, F.; Liang, Y.; Wang, R. Molybdenum Phosphide/Carbon Nanotube Hybrids as pH-Universal Electrocatalysts for Hydrogen Evolution Reaction. *Adv. Funct. Mater.* **2018**, *28* (16). https://doi.org/10.1002/adfm.201706523.

(20) Ge, R.; Huo, J.; Liao, T.; Liu, Y.; Zhu, M.; Li, Y.; Zhang, J.; Li, W. Hierarchical Molybdenum Phosphide Coupled with Carbon as a Whole pH-Range Electrocatalyst for Hydrogen Evolution Reaction. *Appl. Catal. B Environ.* **2020**, *260*, 118196. https://doi.org/10.1016/j.apcatb.2019.118196.

(21) De Trizio, L.; Figuerola, A.; Manna, L.; Genovese, A.; George, C.; Brescia, R.; Saghi, Z.; Simonutti, R.; Van Huis, M.; Falqui, A. Size-Tunable, Hexagonal Plate-like Cu_3P and Janus-like Cu–Cu_3P Nanocrystals. *ACS Nano* **2012**, *6* (1), 32–41. https://doi.org/10.1021/nn203702r.

(22) De Trizio, L.; Gaspari, R.; Bertoni, G.; Kriegel, I.; Moretti, L.; Scotognella, F.; Maserati, L.; Zhang, Y.; Messina, G. C.; Prato, M.; Marras, S.; Cavalli, A.; Manna, L. $Cu_{3-x}P$ Nanocrystals as a Material Platform for Near-Infrared Plasmonics and Cation Exchange Reactions. *Chem. Mater.* **2015**, *27* (3), 1120–1128. https://doi.org/10.1021/cm5044792.

(23) Li, X.; Zhang, J.; Zhang, Y.; Zhang, R.; Chen, D.; Zhang, C.; Zhang, X.; Wang, B.; Luo, H. Q.; Li, N. B. Copper Induced Phosphide for Enhanced Electrochemical Hydrogen Evolution Reaction. *Int. J. Hydrogen Energy* **2020**, *45* (41), 21422–21430. https://doi.org/10.1016/j.ijhydene.2020.05.213.

(24) Sabir, A. S.; Pervaiz, E.; Khosa, R.; Sohail, U. An Inclusive Review and Perspective on Cu-Based Materials for Electrochemical Water Splitting. *RSC Adv.* **2023**, *13* (8), 4963–4993. https://doi.org/10.1039/D2RA07901A.

(25) Perera, S. C.; Tsoi, G.; Wenger, L. E.; Brock, S. L. Synthesis of MnP Nanocrystals by Treatment of Metal Carbonyl Complexes with Phosphines: A New, Versatile Route to Nanoscale Transition Metal Phosphides. *J. Am. Chem. Soc.* **2003**, *125* (46), 13960–13961. https://doi.org/10.1021/ja038037h.

(26) Gregg, K. A.; Perera, S. C.; Lawes, G.; Shinozaki, S.; Brock, S. L. Controlled Synthesis of MnP Nanorods: Effect of Shape Anisotropy on Magnetization. *Chem. Mater.* **2006**, *18* (4), 879–886. https://doi.org/10.1021/cm052080h.

(27) Deng, Q.; Dong, X.; Shen, P. K.; Zhu, J. Li–S Chemistry of Manganese Phosphides Nanoparticles With Optimized Phase. *Adv. Sci.* **2023**, *10* (9). https://doi.org/10.1002/advs.202207470.

(28) Pu, Z.; Liu, Q.; Asiri, A. M.; Sun, X. Tungsten Phosphide Nanorod Arrays Directly Grown on Carbon Cloth: A Highly Efficient and Stable Hydrogen Evolution Cathode at All pH Values. *ACS Appl. Mater. Interfaces* **2014**, *6* (24), 21874–21879. https://doi.org/10.1021/am5060178.

(29) Hong, L.; Guo, R.; Yuan, Y.; Ji, X.; Lin, Z.; Li, Z.; Pan, W. Recent Progress of Transition Metal Phosphides for Photocatalytic Hydrogen Evolution. *ChemSusChem* **2021**, *14* (2), 539–557. https://doi.org/10.1002/cssc.202002454.

(30) Cao, S.; Wang, C.; Fu, W.; Chen, Y. Metal Phosphides as Co-Catalysts for Photocatalytic and Photoelectrocatalytic Water Splitting. *ChemSusChem* **2017**, *10* (22), 4306–4323. https://doi.org/10.1002/cssc.201701450.

(31) Oyama, S. T. Novel Catalysts for Advanced Hydroprocessing: Transition Metal Phosphides. *J. Catal.* **2003**, *216* (1–2), 343–352. https://doi.org/10.1016/S0021-9517(02)00069-6.

(32) Fujita, S.; Nakajima, K.; Yamasaki, J.; Mizugaki, T.; Jitsukawa, K.; Mitsudome, T. Unique Catalysis of Nickel Phosphide Nanoparticles to Promote the Selective Transformation of Biofuranic Aldehydes into Diketones in Water. *ACS Catal.* **2020**, *10* (7), 4261–4267. https://doi.org/10.1021/acscatal.9b05120.

(33) Tsuda, T.; Sheng, M.; Ishikawa, H.; Yamazoe, S.; Yamasaki, J.; Hirayama, M.; Yamaguchi, S.; Mizugaki, T.; Mitsudome, T. Iron Phosphide Nanocrystals as an Air-Stable Heterogeneous Catalyst for Liquid-Phase Nitrile Hydrogenation. *Nat. Commun.* **2023**, *14* (1), 5959. https://doi.org/10.1038/s41467-023-41627-6.

(34) Yamaguchi, S.; Fujita, S.; Nakajima, K.; Yamazoe, S.; Yamasaki, J.; Mizugaki, T.; Mitsudome, T. Air-Stable and Reusable Nickel Phosphide Nanoparticle Catalyst for the Highly Selective Hydrogenation of D-Glucose to D-Sorbitol. *Green Chem.* **2021**, *23* (5), 2010–2016. https://doi.org/10.1039/D0GC03301D.

(35) Downes, C. A.; Libretto, N. J.; Harman-Ware, A. E.; Happs, R. M.; Ruddy, D. A.; Baddour, F. G.; Ferrell, J. R.; Habas, S. E.; Schaidle, J. A. Electrocatalytic CO_2 Reduction over Cu_3P Nanoparticles Generated via a Molecular Precursor Route. *ACS Appl. Energy Mater.* **2020**, *3* (11), 10435–10446. https://doi.org/10.1021/acsaem.0c01360.

(36) Calvinho, K. U. D.; Laursen, A. B.; Yap, K. M. K.; Goetjen, T. A.; Hwang, S.; Murali, N.; Mejia-Sosa, B.; Lubarski, A.; Teeluck, K. M.; Hall, E. S.; Garfunkel, E.; Greenblatt, M.; Dismukes, G. C. Selective CO_2 Reduction to C_3 and C_4 Oxyhydrocarbons on Nickel Phosphides at Overpotentials as Low as 10 mV. *Energy Environ. Sci.* **2018**, *11* (9), 2550–2559. https://doi.org/10.1039/c8ee00936h.

(37) Ji, L.; Li, L.; Ji, X.; Zhang, Y.; Mou, S.; Wu, T.; Liu, Q.; Li, B.; Zhu, X.; Luo, Y.; Shi, X.; Asiri, A. M.; Sun, X. Highly Selective Electrochemical Reduction of CO_2 to Alcohols on an FeP Nanoarray. *Angew. Chemie Int. Ed.* **2020**, *59* (2), 758–762. https://doi.org/10.1002/anie.201912836.

(38) Liu, X.; Cui, C.; Wei, S.; Han, J.; Zhu, X.; Ge, Q.; Wang, H. The Synergy of in Situ-Generated Ni^0 and Ni_2P to Enhance CO Adsorption and Protonation for Selective CH_4 Production from Photocatalytic CO_2 Reduction. *Green Chem.* **2023**, *26* (1), 531–541. https://doi.org/10.1039/d3gc03549b.

(39) Calvinho, K. U. D.; Alherz, A. W.; Yap, K. M. K.; Laursen, A. B.; Hwang, S.; Bare, Z. J. L.; Clifford, Z.; Musgrave, C. B.; Dismukes, G. C. Surface Hydrides on Fe_2P Electrocatalyst Reduce CO_2 at Low Overpotential: Steering Selectivity to Ethylene Glycol. *J. Am. Chem. Soc.* **2021**, *143* (50), 21275–21285. https://doi.org/10.1021/jacs.1c03428.

(40) Li, Y.; Dong, Z.; Jiao, L. Multifunctional Transition Metal-Based Phosphides in Energy-Related Electrocatalysis. *Adv. Energy Mater.* **2020**, *10* (11). https://doi.org/10.1002/aenm.201902104.

(41) Shi, Y.; Zhang, B. Recent Advances in Transition Metal Phosphide Nanomaterials: Synthesis and Applications in Hydrogen Evolution Reaction. *Chem. Soc. Rev.* **2016**, *45* (6), 1529–1541. https://doi.org/10.1039/C5CS00434A.

(42) Aziz, T.; Haque, M. A.; Saha, S.; Mondal, B.; Jain, S.; Dutta, A. A Review of Nanostructured Transition Metal Phosphide-Driven Electrocatalytic Oxygen Evolution Reaction. *Energy & Fuels* **2023**, *37* (23), 18291–18309. https://doi.org/10.1021/acs.energyfuels.3c02773.

(43) Xu, J.; Li, J.; Xiong, D.; Zhang, B.; Liu, Y.; Wu, K.-H.; Amorim, I.; Li, W.; Liu, L. Trends in Activity for the Oxygen Evolution Reaction on Transition Metal (M = Fe, Co, Ni) Phosphide Pre-Catalysts. *Chem. Sci.* **2018**, *9* (14), 3470–3476. https://doi.org/10.1039/C7SC05033J.

(44) You, B.; Jiang, N.; Sheng, M.; Bhushan, M. W.; Sun, Y. Hierarchically Porous Urchin-Like Ni_2P Superstructures Supported on Nickel Foam as Efficient Bifunctional Electrocatalysts for Overall Water Splitting. *ACS Catal.* **2016**, *6* (2), 714–721. https://doi.org/10.1021/acscatal.5b02193.

(45) Joo, J.; Kim, T.; Lee, J.; Choi, S.; Lee, K. Morphology-Controlled Metal Sulfides and Phosphides for Electrochemical Water Splitting. *Adv. Mater.* **2019**, *31* (14). https://doi.org/10.1002/adma.201806682.

(46) Callejas, J. F.; Read, C. G.; Roske, C. W.; Lewis, N. S.; Schaak, R. E. Synthesis, Characterization, and Properties of Metal Phosphide Catalysts for the Hydrogen-Evolution Reaction. *Chem. Mater.* **2016**, *28* (17), 6017–6044. https://doi.org/10.1021/acs.chemmater.6b02148.

(47) Xiao, P.; Chen, W.; Wang, X. A Review of Phosphide-Based Materials for Electrocatalytic Hydrogen Evolution. *Adv. Energy Mater.* **2015**, *5* (24). https://doi.org/10.1002/aenm.201500985.

(48) Zeng, M.; Li, Y. Recent Advances in Heterogeneous Electrocatalysts for the Hydrogen Evolution Reaction. *J. Mater. Chem. A* **2015**, *3* (29), 14942–14962. https://doi.org/10.1039/C5TA02974K.

(49) Carenco, S.; Portehault, D.; Boissière, C.; Mézailles, N.; Sanchez, C. Nanoscaled Metal Borides and Phosphides: Recent Developments and Perspectives. *Chem. Rev.* **2013**, *113* (10), 7981–8065. https://doi.org/10.1021/cr400020d.

(50) Han, S.; Feng, Y.; Zhang, F.; Yang, C.; Yao, Z.; Zhao, W.; Qiu, F.; Yang, L.; Yao, Y.; Zhuang, X.; Feng, X. Metal-Phosphide-Containing Porous Carbons Derived from an Ionic-Polymer Framework and Applied as Highly Efficient Electrochemical Catalysts for Water Splitting. *Adv. Funct. Mater.* **2015**, *25* (25), 3899–3906. https://doi.org/10.1002/adfm.201501390.

(51) Korányi, T. I. Phosphorus Promotion of Ni (Co)-Containing Mo-Free Catalysts in Thiophene Hydrodesulfurization. *Appl. Catal. A Gen.* **2003**, *239* (1–2), 253–267. https://doi.org/10.1016/S0926-860X(02)00390-3.

(52) Liu, Z.; Mu, H.; Xiao, S.; Wang, R.; Wang, Z.; Wang, W.; Wang, Y.; Zhu, X.; Lu, K.; Zhang, H.; Lee, S.; Bao, Q.; Ma, W. Pulsed Lasers Employing Solution-Processed Plasmonic $Cu_{3-x}P$ Colloidal Nanocrystals. *Adv. Mater.* **2016**, *28* (18), 3535–3542. https://doi.org/10.1002/adma.201504927.

(53) Carenco, S.; Resa, I.; Le Goff, X.; Le Floch, P.; Mézailles, N. White Phosphorus as Single Source of "P" in the Synthesis of Nickel Phosphide. *Chem. Commun.* **2008**, No. 22, 2568. https://doi.org/10.1039/b802454e.

(54) Carenco, S.; Hu, Y.; Florea, I.; Ersen, O.; Boissière, C.; Mézailles, N.; Sanchez, C. Metal-Dependent Interplay between Crystallization and Phosphorus Diffusion during the Synthesis of Metal Phosphide Nanoparticles. *Chem. Mater.* **2012**, *24* (21), 4134–4145. https://doi.org/10.1021/cm3022243.

(55) Son, C. Y.; Kwak, I. H.; Lim, Y. R.; Park, J. FeP and FeP_2 Nanowires for Efficient Electrocatalytic Hydrogen Evolution Reaction. *Chem. Commun.* **2016**, *52* (13), 2819–2822. https://doi.org/10.1039/C5CC09832G.

(56) Dutta, A.; Dutta, S. K.; Mehetor, S. K.; Mondal, I.; Pal, U.; Pradhan, N. Oriented Attachments and Formation of Ring-on-Disk Heterostructure Au–Cu_3P Photocatalysts. *Chem. Mater.* **2016**, *28* (6), 1872–1878. https://doi.org/10.1021/acs.chemmater.6b00050.

(57) Inoue, R.; Yamaguchi, M.; Murakami, Y.; Okano, K.; Mori, A. Revisiting of Benzophenone Ketyl Still: Use of a Sodium Dispersion for the Preparation of Anhydrous Solvents. *ACS Omega* **2018**, *3* (10), 12703–12706. https://doi.org/10.1021/acsomega.8b01707.

(58) Schrader, E. Synthesis and Properties of Acylphosphines, ETH Zurich, 2018. https://doi.org/10.3929/ethz-b-000280388.

(59) Scott, D. J.; Cammarata, J.; Schimpf, M.; Wolf, R. Synthesis of Monophosphines Directly from White Phosphorus. *Nat. Chem.* **2021**, *13* (5), 458–464. https://doi.org/10.1038/s41557-021-00657-7.

(60) Muthuswamy, E.; Savithra, G. H. L.; Brock, S. L. Synthetic Levers Enabling Independent Control of Phase, Size, and Morphology in Nickel Phosphide Nanoparticles. *ACS Nano* **2011**, *5* (3), 2402–2411. https://doi.org/10.1021/nn1033357.

(61) Wang, J.; Johnston-Peck, A. C.; Tracy, J. B. Nickel Phosphide Nanoparticles with Hollow, Solid, and Amorphous Structures. *Chem. Mater.* **2009**, *21* (19), 4462–4467. https://doi.org/10.1021/cm901073k.

(62) Chiang, R.-K.; Chiang, R.-T. Formation of Hollow Ni_2P Nanoparticles Based on the Nanoscale Kirkendall Effect. *Inorg. Chem.* **2007**, *46* (2), 369–371. https://doi.org/10.1021/ic061846s.

(63) Henkes, A. E.; Vasquez, Y.; Schaak, R. E. Converting Metals into Phosphides: A General Strategy for the Synthesis of Metal Phosphide Nanocrystals. *J. Am. Chem. Soc.* **2007**, *129* (7), 1896–1897. https://doi.org/10.1021/ja068502l.

(64) Alba-Molina, D.; Puente Santiago, A. R.; Giner-Casares, J. J.; Rodríguez-Castellón, E.; Martín-Romero, M. T.; Camacho, L.; Luque, R.; Cano, M. Tailoring the ORR and HER Electrocatalytic Performances of Gold Nanoparticles through Metal–Ligand Interfaces. *J. Mater. Chem. A* **2019**, *7* (35), 20425–20434. https://doi.org/10.1039/C9TA05492H.

(65) Senevirathne, K.; Burns, A. W.; Bussell, M. E.; Brock, S. L. Synthesis and Characterization of Discrete Nickel Phosphide Nanoparticles: Effect of Surface Ligation Chemistry on Catalytic Hydrodesulfurization of Thiophene. *Adv. Funct. Mater.* **2007**, *17* (18), 3933–3939. https://doi.org/10.1002/adfm.200700758.

(66) Ung, D.; Cossairt, B. M. Effect of Surface Ligands on CoP for the Hydrogen Evolution Reaction. *ACS Appl. Energy Mater.* **2019**, *2* (3), 1642–1645. https://doi.org/10.1021/acsaem.9b00240.

(67) Nag, A.; Kovalenko, M. V.; Lee, J.; Liu, W.; Spokoyny, B.; Talapin, D. V. Metal-Free Inorganic Ligands for Colloidal Nanocrystals: S^{2-}, HS^-, Se^{2-}, HSe^-, Te^{2-}, HTe^-, TeS_3^{2-}, OH^-, and NH_2^- as Surface Ligands. *J. Am. Chem. Soc.* **2011**, *133* (27), 10612–10620. https://doi.org/10.1021/ja2029415.

(68) Liu, W.; Srivastava, V.; Kurley, J. M.; Jiang, C.; Talapin, D. V. Thermal Stability of Semiconductor Nanocrystal Solids: Understanding Nanocrystal Sintering and Grain Growth. *J. Phys. Chem. C* **2022**, *126* (49), 21136–21148. https://doi.org/10.1021/acs.jpcc.2c07400.

(69) Liu, G.; Hou, F.; Peng, S.; Wang, X.; Fang, B. Synthesis, Physical Properties and Electrocatalytic Performance of Nickel Phosphides for Hydrogen Evolution Reaction of Water Electrolysis. *Nanomaterials* **2022**, *12* (17), 2935. https://doi.org/10.3390/nano12172935.

(70) Bandyopadhyay, D.; Ghosh, S.; Houben, L.; Bar-Ziv, R.; Bar-Sadan, M. Full Water Splitting Electrolyzed by Cu–Co Bimetallic Phosphides. *ACS Appl. Energy Mater.* **2023**, *6* (21), 10987–10995. https://doi.org/10.1021/acsaem.3c01761.

(71) Lin-Vien, D.; Colthup, N. B.; Fateley, W. G.; Grasselli, J. G. *The Handbook of Infrared and Raman Characteristic Frequencies of Organic Molecules*; Academic Press: San Diego, 1991. https://doi.org/10.1016/B978-0-08-057116-4.50001-8.

(72) Nakamoto, K. *Infrared and Raman Spectra of Inorganic and Coordination Compounds*; Wiley-Interscience: New York, 1978.

(73) Wang, C.; Chai, L.; Cui, X.; Zhou, Z.; Liu, S. Amorphous/Crystalline Heterostructured Nickel Phosphide Nanospheres for Electrocatalytic Water and Methanol Oxidation Reactions. *J. Phys. Chem. C* **2021**, *125* (39), 21443–21452. https://doi.org/10.1021/acs.jpcc.1c05899.

(74) Beltrán-Suito, R.; Menezes, P. W.; Driess, M. Amorphous Outperforms Crystalline Nanomaterials: Surface Modifications of Molecularly Derived CoP Electro(Pre)Catalysts for Efficient Water-Splitting. *J. Mater. Chem. A* **2019**, *7* (26), 15749–15756. https://doi.org/10.1039/C9TA04583J.

(75) Zhang, H.-M.; Wang, J.-J.; Meng, Y.; Sun, J. Recent Advances in Amorphous Metal Phosphide Electrocatalysts for Hydrogen Evolution Reaction. *Int. J. Hydrogen Energy* **2022**, *47* (85), 36084–36097. https://doi.org/10.1016/j.ijhydene.2022.08.184.

(76) Hu, G.; Tang, Q.; Jiang, D. CoP for Hydrogen Evolution: Implications from Hydrogen Adsorption. *Phys. Chem. Chem. Phys.* **2016**, *18* (34), 23864–23871. https://doi.org/10.1039/C6CP04011J.

(77) Mou, J.; Gao, Y.; Wang, J.; Ma, J.; Ren, H. Hydrogen Evolution Reaction Activity Related to the Facet-Dependent Electrocatalytic Performance of NiCoP from First Principles. *RSC Adv.* **2019**, *9* (21), 11755–11761. https://doi.org/10.1039/C9RA01560D.

(78) Eftekhari, A. Electrocatalysts for Hydrogen Evolution Reaction. *Int. J. Hydrogen Energy* **2017**, *42* (16), 11053–11077. https://doi.org/10.1016/j.ijhydene.2017.02.125.

(79) Shinagawa, T.; Garcia-Esparza, A. T.; Takanabe, K. Insight on Tafel Slopes from a Microkinetic Analysis of Aqueous Electrocatalysis for Energy Conversion. *Sci. Rep.* **2015**, *5* (1), 13801. https://doi.org/10.1038/srep13801.

(80) Paseka, I. Evolution of Hydrogen and Its Sorption on Remarkable Active Amorphous Smooth Ni-P(x) Electrodes. *Electrochim. Acta* **1995**, *40* (11), 1633–1640. https://doi.org/10.1016/0013-4686(95)00077-R.

(81) Bellato, F.; Ferri, M.; Annamalai, A.; Prato, M.; Leoncino, L.; Brescia, R.; De Trizio, L.; Manna, L. Colloidal Synthesis of Nickel Arsenide Nanocrystals for Electrochemical Water Splitting. *ACS Appl. Energy Mater.* **2023**, *6* (1), 151–159. https://doi.org/10.1021/acsaem.2c02698.

(82) Mahmood, N.; Yao, Y.; Zhang, J.; Pan, L.; Zhang, X.; Zou, J. Electrocatalysts for Hydrogen Evolution in Alkaline Electrolytes: Mechanisms, Challenges, and Prospective Solutions. *Adv. Sci.* **2018**, *5* (2), 1700464. https://doi.org/10.1002/advs.201700464.

(83) Read, C. G.; Callejas, J. F.; Holder, C. F.; Schaak, R. E. General Strategy for the Synthesis of Transition Metal Phosphide Films for Electrocatalytic Hydrogen and Oxygen Evolution. *ACS Appl. Mater. Interfaces* **2016**, *8* (20), 12798–12803. https://doi.org/10.1021/acsami.6b02352.

(84) Zhang, R.; Wang, X.; Yu, S.; Wen, T.; Zhu, X.; Yang, F.; Sun, X.; Wang, X.; Hu, W. Ternary $NiCo_2P_x$ Nanowires as pH-Universal Electrocatalysts for Highly Efficient Hydrogen Evolution Reaction. *Adv. Mater.* **2017**, *29* (9), 1605502. https://doi.org/10.1002/adma.201605502.